Shifted resonances in coated metamaterial cylinders: Enhanced backscattering and near-field effects

C. W. Qiu,[1,2,*] S. Zouhdi,[1] and Y. L. Geng[3]
[1]*Laboratoire de Génie Electrique de Paris, École Supérieure D'Électricité, LGEP-SUPELEC, Plateau de Moulon 91192, Gif-Sur-Yvette, France*
[2]*Department of Electrical and Computer Engineering, National University of Singapore, 4 Engineering Drive 3, 117576 Singapore*
[3]*Institute of Antenna and Microwaves, Hangzhou Dianzi University, Hangzhou, Zhejiang, 310018 China*
(Received 11 September 2007; published 14 April 2008)

Electromagnetic wave properties in the presence of a thin or thick coating on a cylinder are investigated. The theoretical treatment starts from the formulation of electromagnetic fields in all regions where the coating and the core are allowed to rotate. The angular velocities of the core and coating can be different and even antidirectional. The present general approach can be applied to a wide range of specific cases such as rotating and stationary and left-handed and right-handed core-coating combinations. In particular, the optical resonances due to the surface plolaritons and morphology-dependent resonances are examined. Because of the rotation, the resonances are found to shift, and the effects of velocity on such phenomena are investigated. The backscattering can thus be controlled to achieve suppression or enhancement by using proper metamaterial coatings. Physical insights as well as the numerical results are presented.

DOI: 10.1103/PhysRevE.77.046604 PACS number(s): 03.50.De, 42.70.−a, 42.50.Gy, 33.20.Fb

I. INTRODUCTION

The scattering and diffraction of electromagnetic waves by composite cylinders have been discussed comprehensively [1]. Later, a study of scattering off a cylinder with an inhomogeneous coating was carried out [2], and plasma-coated cylinders were further investigated [3,4]. Various methods have been developed to treat canonical problems, such as the geometric optics method [5,6], dyadic Green's functions [7,8], and multilayer algorithms [9,10]. More recently, the theoretical study of coatings has intensified since the pioneering work by Pendry *et al.* [11,12]. In their work, a *coated* structure can be defined as a target object (penetrable or impenetrable) clad with an electromagnetic material which does not perturb the external fields [11]. This idea of coating has been further employed to achieve transparency by using plasmonic resonances [13,14], full-wave analysis with mixing theory for spheres [16,17], and parallel-plate ϵ-negative materials [18].

On the other hand, theoretical investigation [12,19,20] has revealed that the refractive indices and material parameters of the cloaking structures have to be inhomogeneous, depending on position. Although the approach of conformal mapping can be applied to cases of arbitrary dimension and wavelength, independent control of each element of permittivity and permeability of anisotropic media is necessary, which is difficult to realize invisibility. However, the development of metamaterials and artificial complex materials [21,22] made it possible to significantly reduce the radar cross section (RCS) of a given object [13,15]. Then let us consider coating with RCS reduction, because it is of great importance in radar detection and stealth technology. One can study different combinations of the core and coated layers, among which some unprecedented physical properties and functionalities can be attained. Coatings such as Salisbury or Dallenbach screens [23] have been commonly used to diminish reflection or scattering for decades. In order to increase the bandwidth of RCS reduction, multilayered Salisbury screens [24] were developed, where the highly absorbing bandwidth is proportional to the number of layers, and chiral Dallenbach shields [25,26] were also used since the chirality provides another degree of freedom to reduce the RCS. Metamaterials have been employed in a recent work on coating using a different mechanism, the unusual photon tunneling [27] which is unattainable in conventional materials, such as negative refraction. It is well known that surface polaritons can be generated at an interface between two different materials if the dielectric function of one medium is opposite to, or conjugate with, that of the other within a particular frequency range [28,29]. Those aforementioned shields and bilayers are either based on the absorption mechanism or are only suitable for planar (or nearly planar) objects. The pioneering work by Alù and Engheta [13] demonstrated how a coated spherical object could be made transparent to electromagnetic waves by the use of plasmonic covers mounted on a dielectric core. The scattering cross section can be drastically reduced if the parameters of the materials and the geometry are properly chosen.

In this paper, we continue to discuss these coated structures but primarily focus on cylindrical coating with composite materials. In order to obtain a complete picture of coating effects on RCS reduction, a wide range of core-shell pairings and sizes is explored. Moreover, the rotation effects on the scattering are taken into account, providing some physical insights into the designs of polariton-resonant cylindrical devices [30]. Analytical solutions for the field components in all regions have been explicitly derived, where the rotation factors are incorprated. Numerical results of particular core-shell pairings are presented, showing how the resonant scattering of electrically small coated cylinders is modified by the velocity and size. The present theory is also extended to

*Corresponding author. eleqc@nus.edu.sg

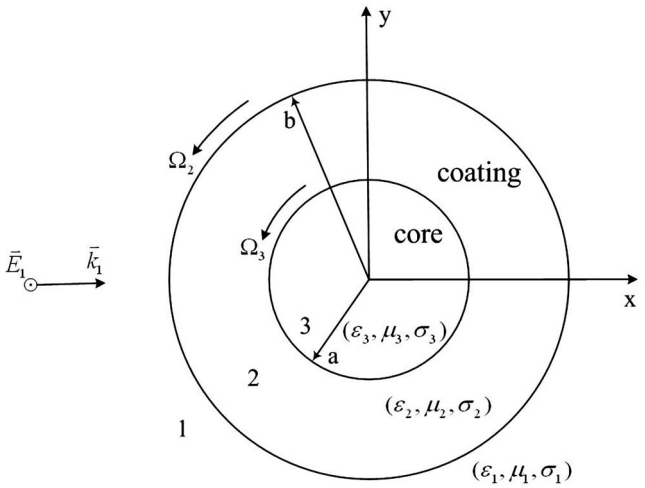

FIG. 1. Geometry of plane-wave scattering by a rotating concentric cylinder.

rotating coatings at electrically large size, where morphology-dependent resonances (MDRs) are presented and discussed. Finally, the findings and results are summarized.

II. PRELIMINARIES

The geometry of the investigated concentric cylinder immersed in a host is shown in Fig. 1. The case of E polarization is considered as the illumination

$$\boldsymbol{E}^i = \hat{z}e^{ik_i x}; \tag{1}$$

the material in each region of Fig. 1 is homogeneous and rotating, and can be characterized by its electric response (ϵ), magnetic response (μ), and angular velocity (Ω). The constitutive relations for a general rotating materials can be formulated [31]

$$\boldsymbol{D} - n^2\beta^2\boldsymbol{D}_\perp = \epsilon(\boldsymbol{E} - \beta^2\boldsymbol{E}_\perp) + \frac{\mu_r\epsilon_r - 1}{c^2}\boldsymbol{v}\times\boldsymbol{H}, \tag{2}$$

$$\boldsymbol{B} - n^2\beta^2\boldsymbol{B}_\perp = \mu(\boldsymbol{H} - \beta^2\boldsymbol{H}_\perp) - \frac{\mu_r\epsilon_r - 1}{c^2}\boldsymbol{v}\times\boldsymbol{E}, \tag{3}$$

$$\boldsymbol{J} = \rho\boldsymbol{v} + \sigma\sqrt{1-\beta^2}\boldsymbol{E}_\parallel + \frac{\sigma}{\sqrt{1-\beta^2}}(\boldsymbol{E}_\perp + \boldsymbol{v}\times\boldsymbol{B}), \tag{4}$$

where σ denotes the conductivity in the corresponding layer, $\boldsymbol{v}=\Omega\rho\hat{\boldsymbol{\phi}}$ represents the rotating velocity, μ_r (ϵ_r) stands for the relative permeability (permittivity), $\beta=\Omega\rho/c$ denotes the normalized velocity, and $\perp$ ($\parallel$) denotes the perpendicular (parallel) component with respect to the axial direction.

Throughout this paper, the time dependence $e^{-i\omega t}$ and small angular velocity are assumed for the instantaneous rest-frame theory [32] so that the term β^2 can be neglected. For the incident wave discussed here, the boundary conditions are

$$\hat{\boldsymbol{\rho}}\cdot(\boldsymbol{D}^{\mathrm{sca}} + \boldsymbol{D}^i - \boldsymbol{D}^t) = \rho_s, \tag{5}$$

$$\hat{\boldsymbol{\rho}}\times(\boldsymbol{H}^{\mathrm{sca}} + \boldsymbol{H}^i - \boldsymbol{H}^t) = J_s. \tag{6}$$

Note that the surface current J_s and surface charge ρ_s are zero, implied by the E polarization, the above boundary conditions, and Eqs. (2) and (3). Hence, the material relations (especially for the current) can be reformulated when small angular velocity is assumed so as to assure applicability of the instantaneous rest-frame theory,

$$\boldsymbol{D} = \epsilon\boldsymbol{E} + \frac{\mu_r\epsilon_r - 1}{c^2}\boldsymbol{v}\times\boldsymbol{H}, \tag{7}$$

$$\boldsymbol{B} = \mu\boldsymbol{H} + \frac{\mu_r\epsilon_r - 1}{c^2}\boldsymbol{E}\times\boldsymbol{v}, \tag{8}$$

$$\boldsymbol{J} = \sigma\boldsymbol{E} + \sigma\mu\boldsymbol{v}\times\boldsymbol{H}. \tag{9}$$

III. THEORETICAL FORMULATION

The incident wave $\boldsymbol{E}^i = E_1^i\hat{z}$ in Eq. (1) can be expressed in the form

$$E_1^i = \sum_{-\infty}^{\infty} i^n J_n(k_1\rho)e^{in\phi} \tag{10}$$

where

$$k_1^2 = \omega^2\epsilon_1\mu_1 + i\omega\sigma_1\mu_1. \tag{11}$$

In the theory of this paper, the outer region can be any dielectric or conducting material. For simplicity of calculation, we just put $\epsilon_1=\epsilon_0$, $\mu_1=\mu_0$, and $\sigma_1=0$, and thus $k_1^2=\omega^2\epsilon_1\mu_1 = \omega^2\epsilon_0\mu_0$. It follows that scattered field in the first region must have the form

$$E_1^{\mathrm{sca}} = \sum_{-\infty}^{\infty} i^n A_n H_n^{(1)}(k_1\rho)e^{in\phi}. \tag{12}$$

First, let us discuss the eigenwave number in a rotating wire. From Eqs. (7)–(9), the following equations for transmitted waves can be obtained:

$$\frac{1}{\rho}\frac{\partial E_z^t}{\partial\phi} = i\omega\mu H_\rho^t - i\omega\Omega\rho\frac{\mu_r\epsilon_r - 1}{c^2}E_z^t, \tag{13}$$

$$-\frac{\partial E_z^t}{\partial\rho} = i\omega\mu H_\phi^t, \tag{14}$$

$$\frac{1}{\rho}\frac{\partial}{\partial\rho}(\rho H_\phi^t) - \frac{1}{\rho}\frac{\partial H_\rho^t}{\partial\phi} = (\sigma - i\omega\epsilon)E_z^t - \Omega\rho\left(\sigma\mu - i\omega\frac{\mu_r\epsilon_r - 1}{c^2}\right)H_\rho^t. \tag{15}$$

In general, the transmitted electric fields in regions 2 and 3 can be expressed by the Fourier terms

$$E_z^t = \sum_{-\infty}^{\infty} U_n e^{in\phi}, \tag{16}$$

where U_n is found to satisfy

$$\frac{1}{\partial\rho}\frac{\partial}{\partial\rho}\left(\rho\frac{\partial U_n}{\partial\rho}\right)+\left(k_{nq}^2-\frac{n^2}{\rho^2}\right)U_n=0. \tag{17}$$

Equation (17) is actually a definition of Bessel functions and thus Eq. (16) becomes

$$E_z^t=\sum_{-\infty}^{\infty} i^n\Lambda_q J_n(k_{nq}\rho)e^{in\phi}, \tag{18}$$

where i^n is inherited from the incident wave, Λ_q represents the unknown scattering coefficient, $q=2$ or 3 stands for the region number, and

$$k_{nq}^2=\omega^2\epsilon_q\mu_q+i\omega\mu_q\sigma_q+\frac{n\Omega_q\omega}{c^2}\left(2\epsilon_{rq}\mu_{rq}-2+i\frac{\sigma_q\mu_{rq}}{\omega\epsilon_0}\right). \tag{19}$$

After applying the boundary condition at the inner interface, one can obtain the transmitted fields in regions 2 and 3 in Fig. 1:

$$E_2=\sum_{-\infty}^{\infty} i^n[B_nH_n^{(2)}(k_{n2}\rho)+C_nH_n^{(1)}(k_{n2}\rho)]e^{in\phi}, \tag{20}$$

$$E_3=\sum_{-\infty}^{\infty} i^nD_nJ_n(k_{n3}\rho)e^{in\phi}, \tag{21}$$

where the superscripts (1) and (2) denote Hankel functions of the first and second type, respectively.

Thus, the boundary matching at $\rho=a$ and $\rho=b$ is performed for E_z and H_ϕ [see Eq. (14)]. One can obtain the following scattering coefficients after a long algebraic calculation:

$$A_n=\frac{(\mu_{r2}/\mu_{r1})\Delta_nJ_n'(k_1b)-(k_{n2}/k_1)\Pi_nJ_n(k_1b)}{(k_{n2}/k_1)\Pi_nH_n^{(1)}(k_1b)-(\mu_{r2}/\mu_{r1})\Delta_nH_n'^{(1)}(k_1b)}, \tag{22}$$

$$B_n=P_nC_n, \tag{23}$$

$$C_n=\frac{-\frac{2i}{\pi(k_1b)}\frac{\mu_{r2}}{\mu_{r1}}}{\frac{k_{n2}}{k_1}\Pi_nH_n^{(1)}(k_1b)-\frac{\mu_{r2}}{\mu_{r1}}\Delta_nH_n'^{(1)}(k_1b)}, \tag{24}$$

$$D_n=\frac{\frac{8}{\pi^2(k_1b)(k_{n2}a)}\frac{\mu_{r3}}{\mu_{r1}}}{\frac{k_{n3}}{k_{n2}}J_n'(k_{n3}a)H_n^{(2)}(k_{n2}a)-\frac{\mu_{r3}}{\mu_{r2}}J_n(k_{n3}a)H_n'^{(2)}(k_{n2}a)}\times\frac{1}{\frac{k_{n2}}{k_1}\Pi_nH_n^{(1)}(k_1b)-\frac{\mu_{r2}}{\mu_{r1}}\Delta_nH_n'^{(1)}(k_1b)}, \tag{25}$$

where Wronskians have been used, and

$$\Delta_n=H_n^{(2)}(k_{n2}b)P_n+H_n^{(1)}(k_{n2}b), \tag{26}$$

$$\Pi_n=H_n'^{(2)}(k_{n2}b)P_n+H_n'^{(1)}(k_{n2}b), \tag{27}$$

$$P_n=\frac{\frac{\mu_{r3}}{\mu_{r2}}J_n(k_{n3}a)H_n'^{(1)}(k_{n2}a)-\frac{k_{n3}}{k_{n2}}J_n'(k_{n3}a)H_n^{(1)}(k_{n2}a)}{\frac{k_{n3}}{k_{n2}}J_n'(k_{n3}a)H_n^{(2)}(k_{n2}a)-\frac{\mu_{r3}}{\mu_{r2}}J_n(k_{n3}a)H_n'^{(2)}(k_{n2}a)}. \tag{28}$$

Note that the derivatives are all with respect to the argument.

The backscattering cross section is defined as the ratio of power scattered directly back toward the source to the incident power per unit area,

$$\sigma_B=\frac{4}{k_1}\left|\sum_{n=0}^{\infty}(2-\delta_n^0)(-1)^nA_n\right|^2, \tag{29}$$

where δ_n^0 is the Kronecker delta function.

In all calculations, we use the identity of the backscattering cross section $C_B=\sigma_B/b$, which is normalized by the physical size of the outer radius b.

IV. COATING WITH DIELECTRIC MATERIALS

In this section, we first consider a stationary core with a rotating coating. Assume that the core layer is made of a conventional dielectric ($\epsilon_{r3}=2$, $\mu_{r3}=1$) and the coating is a left-handed material (LHM) characterized by $\epsilon_{r2}=-2$ and $\mu_{r2}=-1$ with a velocity of $\beta_2=\frac{\Omega_2 b}{c}$. In order to satisfy the first-order theory, it implies that $\beta_2\ll 1$ so that β_2^2 can be neglected [32]. Therefore, k_{n2} in Eq. (19) can be rewritten as

$$k_{n2}\approx k_1N_2+\beta_2\frac{N_2^2-1}{N_2}\frac{n}{b}, \tag{30}$$

$$N_2=\sqrt{\epsilon_{r2}}\sqrt{\mu_{r2}}. \tag{31}$$

Note that for the antivacuo (i.e., left-handed vacuum) coating, the rotation of the coating has no effect on the scattering properties since the second term in Eq. (30) disappears. For the dielectric case, the calculations will be much simplified if the small-argument asymptotic forms of various Bessel and Hankel functions are employed.

Of particular interest is the conjugate pair of μ-negative (MNG) and ϵ-negative (ENG) materials. It has been shown that surface polaritons can be generated at the interface between MNG and ENG layers [27]. We study two cases of such core-shell pairings with the sequences of MNG-ENG and ENG-MNG.

As shown in Fig. 2, the coated cylinder has optical size of $k_1b=0.001$. In the first case, Fig. 2(a), the coating is made of the ENG material ($\epsilon_2=-3\epsilon_0$ and $\mu_2=4\mu_0$) and the core is filled with the MNG material ($\epsilon_3=\epsilon_0$ and $\mu_3=-2\mu_0$). Another type of conjugate pair (i.e., the core is filled by the ENG material and the coating is the MNG material) is considered in Fig. 2(b) as a complementary case. We keep the absolute values of parameters unchanged as in Fig. 2(a) with only the change in plus and minus signs. One can see that resonance will arise at a particular ratio of radii only if the core and coating are respectively filled by conjugate materials. We plot only a small range of the ratio in the vicinity of resonance, because the resonance is quite sensitive to the ratio when the coaxial wire is of optical size. In fact, we need

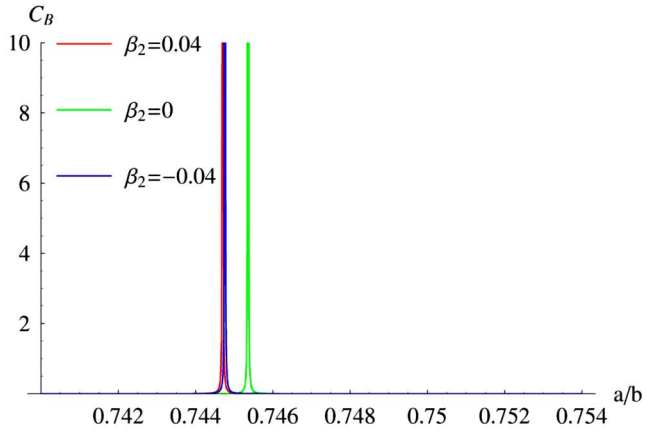

(a) MNG-ENG for the core-coating pair

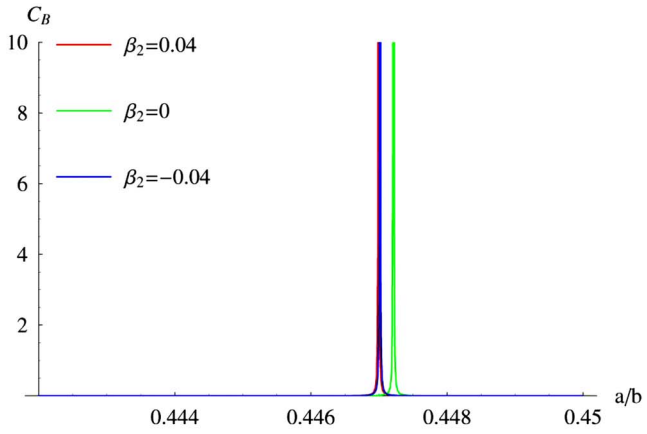

(b) ENG-MNG for the core-coating pair

FIG. 2. (Color online) Normalized backscattering and resonance of conjugate optical coating for $k_1b=0.001$ at different velocities with a stationary core. The first region is free space. (a) ENG coating, $\epsilon_2=-3\epsilon_0$, $\mu_2=4\mu_0$, and MNG core, $\epsilon_3=\epsilon_0$, $\mu_3=-2\mu_0$; (b) MNG coating $\epsilon_2=3\epsilon_0$, $\mu_2=-4\mu_0$, and ENG core, $\epsilon_3=-\epsilon_0$, $\mu_3=2\mu_0$.

to plot the resonance in A_n in Eq. (22) first over the whole range (0,1). Since the resonance in A_n is less sensitive and easier to observe, the resonant position can be approximated first, and then the backscattering cross section C_B is plotted by using proper steps within the particular range. Otherwise, such resonant phenomena are very likely to be missed. In Fig. 2(a), two rotating coatings with opposite directions (one is along $\hat{\phi}$ and the other is along $-\hat{\phi}$) are considered and compared with the stationary case. It shows that, if the coating is stationary, the resonance occurs at the ratio at $a/b \approx 0.7454$. Once the coating has a small rotating velocity (e.g., ± 0.04), the original resonance will disappear and be shifted to $a/b \approx 0.7448$ instead. Apart from this region, the value of C_B is negligible. It is found that the direction of the velocities is not important and, if the absolute speeds are the same, they have equivalent effects on the backscattering cross section.

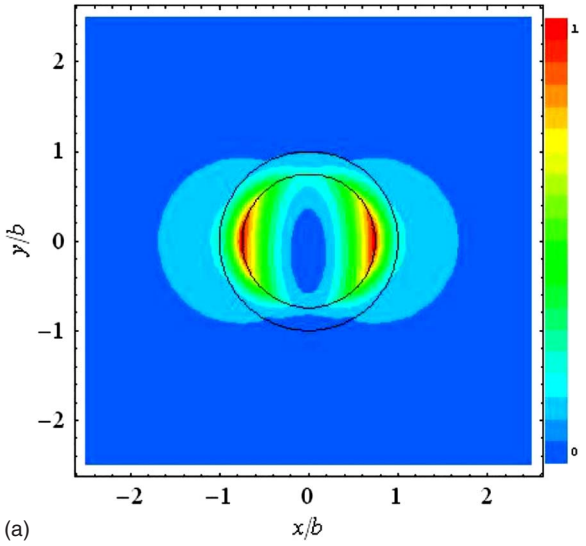

(a)

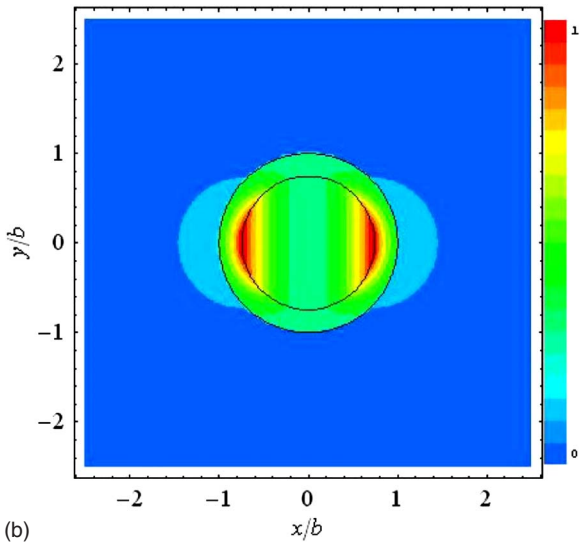

(b)

FIG. 3. (Color online) Contour plots of the distribution of the magnitude of scattered electric components in the x-y plane at the ratio of $a/b=0.745$ with the same ENG coating ($\epsilon_2=-3\epsilon_0$ and $\mu_2=4\mu_0$) and MNG core ($\epsilon_3=\epsilon_0$ and $\mu_3=-2\mu_0$) as in Fig. 2(a). The color in the plot has been scaled by its maximum value.

It is also found that the resonant characteristics are greatly modified in Fig. 2(b) compared with Fig. 2(a), and stationary resonance occurs at $a/b \approx 0.447$ while rotation shifts the resonance to $a/b \approx 0.4473$. One finds that the rotation resonances always arise below the stationary resonances for conjugate pairs of core and coating at optical size. Further simulations reveal that the introduction of loss in the coating will not affect the position of the resonant shift due to the rotation, but the resonant magnitudes for both stationary and rotating cases in Fig. 2 will be reduced, as expected, with increased loss.

In Fig. 3, the electric field distribution is shown. The incident plane wave is propagating along the $\hat{x}$ direction with the electric field polarized along $\hat{z}$. Localization of the energy of the electric fields occurs at the interface between the core and the coating. Resonances due to surface plasmon polari-

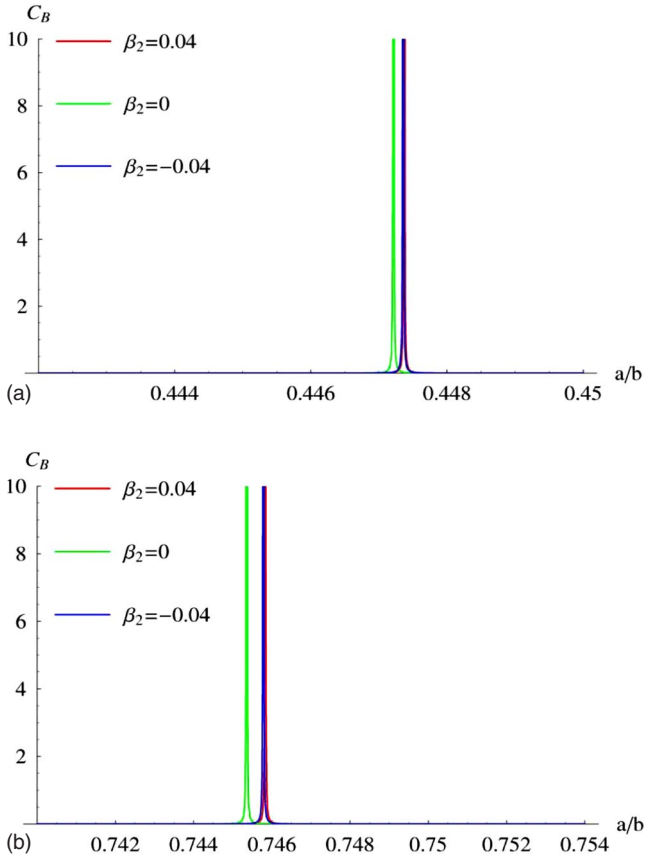

FIG. 4. (Color online) Normalized backscattering and resonance of LHM (RHM) optical coating for $k_1b=0.001$ at different velocities with a stationary RHM (LHM) core. (a) LHM coating, $\epsilon_2=-3\epsilon_0$, $\mu_2=-4\mu_0$, and RHM core, $\epsilon_3=\epsilon_0$, $\mu_3=2\mu_0$; (b) RHM coating, $\epsilon_2=3\epsilon_0$, $\mu_2=4\mu_0$, and LHM core, $\epsilon_3=-\epsilon_0$, $\mu_3=-2\mu_0$.

tons arise, as expected, at the input and output windows. The rotation of the coating, though not very fast, markedly modifies the energy distribution inside the concentric cylinder. It can be seen that the slow rotation of the coating confines the localization and surface polaritons in more restricted input and output windows. The distribution pattern of the rotationary case remains analogous to that of the stationary case, except for the whirlpool at the center of the inner core. Further simulations when the ratio of a/b is not in the vicinity of 0.7448 under the same conditions as in Fig. 3(a) reveal that the resonances will never arise at any position inside the coated cylinder.

In contrast to the conjugate pairing in Fig. 2, the situation will be very different for a pair of left-handed and right-handed materials (RHMs). Two core-coating combinations are studied: (1) the core is a RHM and the coating is a LHM; and (2) the core is a LHM and the coating is a RHM. In Fig. 4, one can see that the rotation resonances are always above the stationary resonances. It also agrees with the results in Fig. 2 that the rotation of the coating shifts the resonant position and oppositely rotating directions lead to identical results. More interestingly, let us examine Fig. 2(a) along with Fig. 4(b). It is evident that those two cases (i.e., the conjugate pair and LHM-RHM pair) are quite similar. The stationary resonances appear at the same ratio, but the rotation of the coating leads to a different contribution to the resonance shift. An analogous phenomenon can be found in Fig. 2(b) along with Fig. 4(a). In addition to the far-field diagrams, the contour plot of the distribution of the electric field magnitude in the near zone is presented in Fig. 5 where the LHM coating and RHM core are characterized by $\epsilon_2=-3\epsilon_0$, $\mu_2=-4\mu_0$ and $\epsilon_3=\epsilon_0$, $\mu_3=2\mu_0$, respectively. The localization of the energy at a resonant scattering ratio of 0.447 can be seen. This again confirms that surface polaritons can be excited in TM incidence by judicious selection of materials and ratios of the core and coating. In the stationary case, the symmetry of the distribution is preserved, as expected.

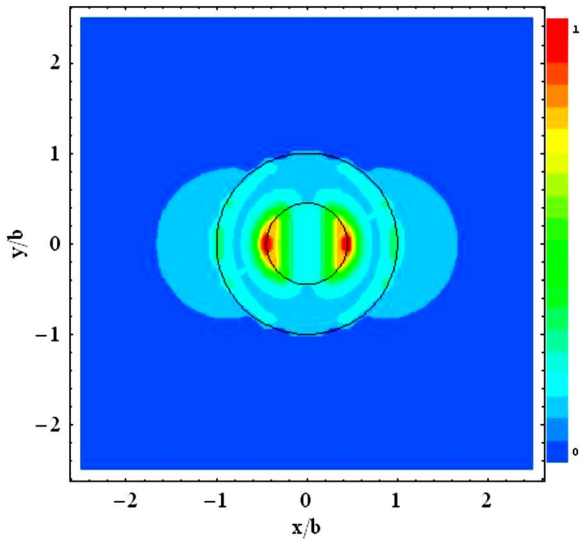

FIG. 5. (Color online) Distribution of the magnitude of the electric field in the stationary case when the ratio of a/b is 0.447. The materials in the inner and outer layers are the same as those in Fig. 4(a). The color has been scaled by its maximum value.

By comparing Fig. 6 with Fig. 5, the effect of rotation seems obvious: the field inside the cylinder can be enhanced even if the rotation of the coating is very slow. his may be explained in terms of the field lines of the Poynting vector [33] (i.e., more Poynting vector field lines are bent to flow back into the cylinder). When the angular velocity is larger, the field enhancement and the asymmetry of the distribution are more remarkable as shown in Fig. 6.

Next, a LHM coating for thick cylinders is presented in Fig. 7. Two cases of thick cylinders are presented and the materials in each region are positive. When the physical thickness is comparable to the wavelength (i.e., $k_1b=4$), oscillations occur with several peak values as shown in Fig. 7(a). The effects of the rotating velocities and directions become remarkable; the resonant peaks for clockwise rotation are always ahead of those of the stationary case, while the counterclockwise case comes after the stationary case. When the physical thickness is further increased (i.e., $k_1b=20$), multiple resonances can be observed when the ratio is bigger than 0.2 as shown in Fig 7(b). One can find that the resonant scattering amplitude of a thick cylinder coating is reduced when the thickness k_1b increases. In addition, by comparing Fig. 7 with Fig. 4, one can see that the electric size plays an important role in the coating, and is dominated by different

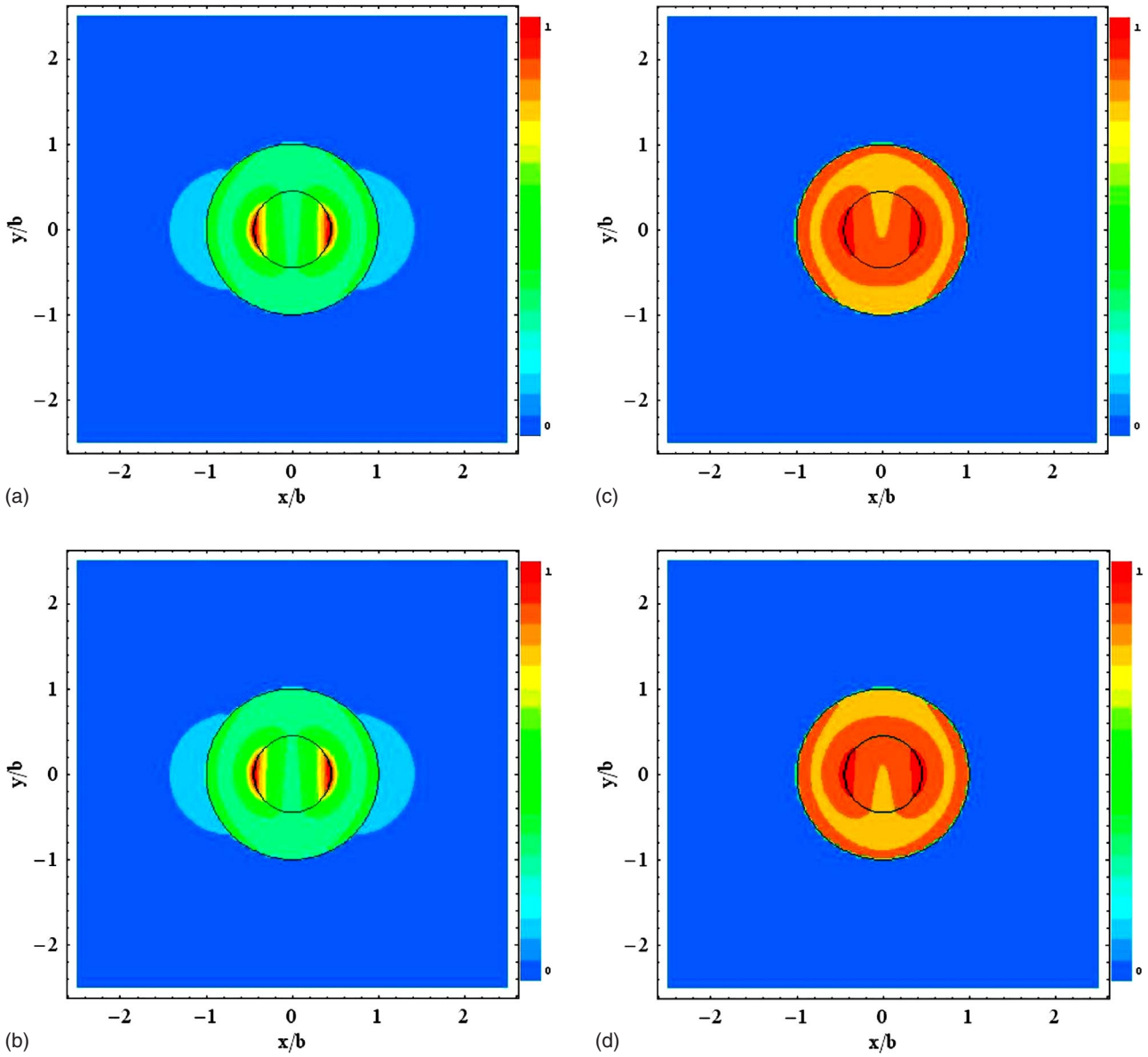

FIG. 6. (Color online) Distribution of the magnitude of the electric field when the coating is rotating at different velocities at $a/b=0.447$. The material, the same as in Fig. 4(a), is characterized by $\epsilon_3=\epsilon_0$, $\mu_3=2\mu_0$ in the inner layer, and by $\epsilon_2=-3\epsilon_0$, $\mu_2=-4\mu_0$ in the coating.

physics. Specifically, for optical coating, the resonances occur mainly because of the existence of surface plasmons at the interface between the core and shell layers. In contrast, morphology-dependent resonances occur for large size as shown in Fig. 7. MDRs are not related to bulk excitations and do not require negative values of the dielectric response, but are determined by the electric size of the scatterer.

In Fig. 8, the core is conventional like that in Fig. 7(b), but the coating is a LHM material. It shows that the change of the coating from a conventional to a LHM will increase the number of points of zero reflection but has no obvious influence on the amplitude at resonance. This effect would be of great use in radar detection and stealth technology, since the cross section can be significantly reduced via easy control of the thickness of an appropriate LHM coating.

V. COATING WITH METALLIC MATERIALS

In this section, the application is extended to metallic coatings. Given $\sigma_q/\omega\epsilon_0=x_q$, Eq. (19) can be rewritten as

$$k_{n2}^2 = k_1^2 N_2^2 + 2n\beta_2 \frac{k_1}{b}(N_2^2 - 1) + i\left(k_1^2 + 2n\beta_2 \frac{k_1}{b}\right)\mu_{r2}x_2, \tag{32}$$

$$k_{n3}^2 = k_1^2 N_3^2 + 2n\beta_3 \frac{k_1}{a}(N_3^2 - 1) + i\left(k_1^2 + 2n\beta_3 \frac{k_1}{a}\right)\mu_{r3}x_3. \tag{33}$$

Hence, the role of the conductivity of the coating in backscattering can be examined. No optical resonances are found

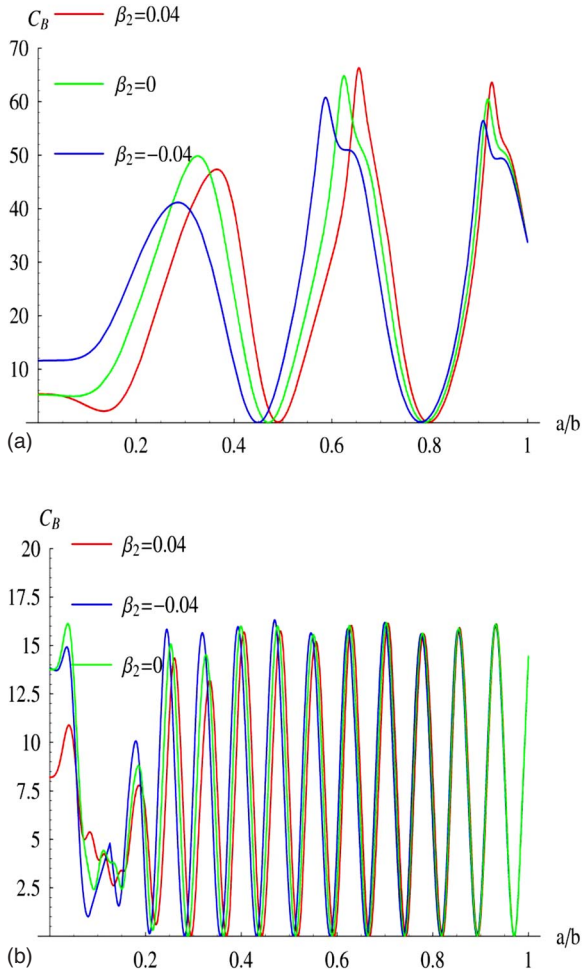

FIG. 7. (Color online) Normalized backscattering and resonance of conventional coating for thick cylinders at different velocities. The materials in core and coating are both conventional. Materials in regions 1 and 3 are the same as in Fig. 4(a) but the second region is different (i.e., $\epsilon_2=3\epsilon_0$, $\mu_2=4\mu_0$ for the coating and $\epsilon_3=\epsilon_0$, $\mu_3=2\mu_0$ for the core). (a) $k_1b=4$ and (b) $k_1b=20$.

for different ratios of a/b, thus the application of metallic coating at small sizes is limited. Instead, we consider only the thick cylinder. First, it is assumed that both layers are metals. The difference between the two conductivities is defined as the ratio σ_3/σ_2. In Fig. 9, the ratio of a/b is set to be 0.8 and the conductivity in the coating is fixed, so as to examine how the difference of the conductivities between core and coating affects the scattering properties. Interestingly, it is found that only when the contrast in conductivities is below 10 is the backscattering greatly modified. The rotation velocity has little influence on the scattering properties for coating of thick conducting cylinders, which is very similar to the stationary case. This is because the case of thick cylinders is approaching the planar case and slow angular rotation has little effect on a flat face.

Regarding the conducting materials, there are two limiting cases within the scope of this paper: (1) the inner cylinder is perfectly electric conductor (PEC); (2) the coating is PEC. As for the second case, it just reduces to a conventional problem, since waves cannot enter into the inner layer.

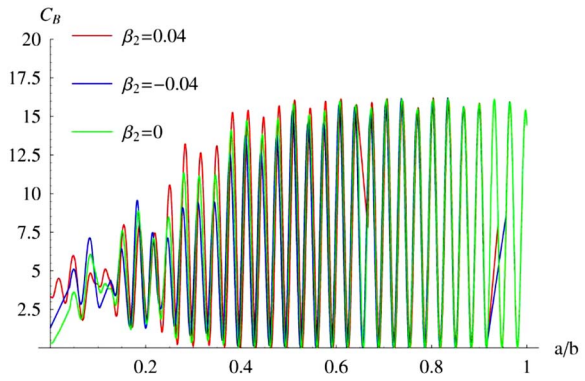

FIG. 8. (Color online) Normalized backscattering and resonance of LHM coating for thick cylinders of $k_1b=20$. The material in the core is the same as Fig. 7 (i.e., $\epsilon_3=\epsilon_0$, $\mu_3=2\mu_0$), while the coating is a left-handed material with $\epsilon_2=-3\epsilon_0$, $\mu_2=-4\mu_0$.

Hence, we can actually treat this case as a PEC cylinder with the radius of b. The scattered wave is thus obtained by reapplying the boundary conditions only at $\rho=b$,

$$E_1^{\text{sca}} = -\sum_{-\infty}^{\infty} i^n J_n(k_1 b)\frac{H_n^{(1)}(k_1\rho)}{H_n^{(1)}(k_1 b)}e^{in\phi}. \tag{34}$$

The solution in Eq. (34) is well known. However, the first case is of particular interest. If the material in $0<\rho<a$ is a perfect electric conductor, the coefficient D_n in Eqs. (21) and (25) is zero, and Eq. (22) becomes

$$\check{A}_n = \frac{k_{n2}J_n(k_1 b)\check{\Delta}_n - k_1 J_n'(k_1 b)\check{\Pi}_n}{k_1 H_n'^{(1)}(k_1 b)\check{\Pi}_n - k_{n2}H_n^{(1)}(k_1 b)\check{\Delta}_n}, \tag{35}$$

where

$$\check{\Delta}_n = H_n'^{(1)}(k_{n2}b)H_n^{(2)}(k_{n2}a) - H_n'^{(2)}(k_{n2}b)H_n^{(1)}(k_{n2}a), \tag{36}$$

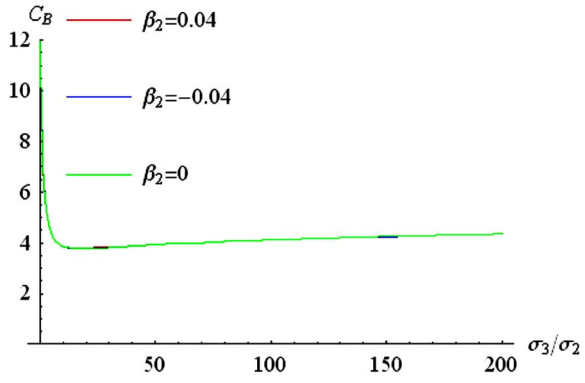

FIG. 9. (Color online) Normalized backscattering versus the conductivity contrast for the coating of thick metallic cylinders of $k_1b=20$. Coating layer: loss tangent is 0.06 (i.e., $x_2=0.03$), and $\epsilon_2=4$. In the core layer $\epsilon_3=2$.

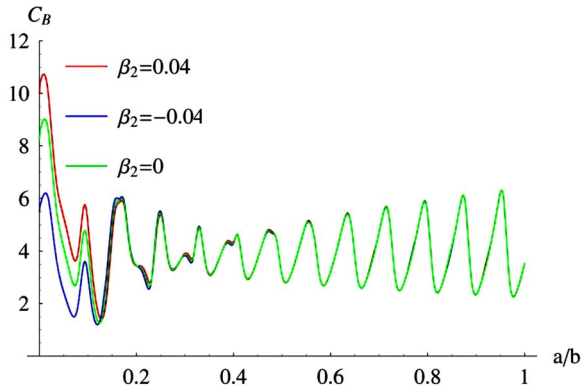

FIG. 10. (Color online) Normalized backscattering versus the ratio of inner to outer radius for thick metallic cylinders of $k_1 b = 20$. The coating material is the same as in Fig. 9 (i.e., loss tangent is 0.06 and $\epsilon_2 = 4$.) but the core is made of PEC.

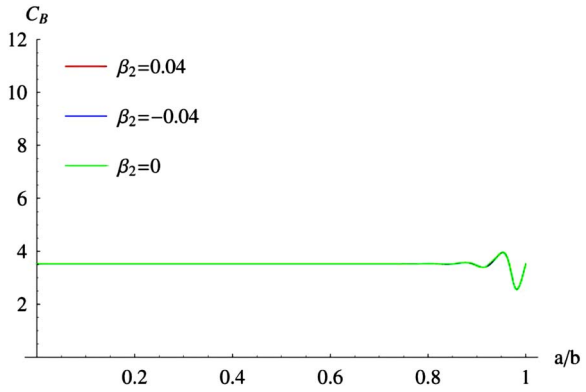

FIG. 11. (Color online) Normalized backscattering versus the ratio of inner to outer radius for thick metallic cylinders of $k_1 b = 20$. Coating layer: loss tangent is 6 (i.e., $x_2 = 3$), and $\epsilon_2 = 4$. Core: PEC.

$$\check{\Pi}_n = H_n^{(1)}(k_{n2}b)H_n^{(2)}(k_{n2}a) - H_n^{(2)}(k_{n2}b)H_n^{(1)}(k_{n2}a). \quad (37)$$

In Figs. 10 and 11, we consider PEC cores coated with low- and high-loss material, respectively. In Fig. 10, the angular velocity gives little contribution to the backscattering when $a < 0.15b$. Only when the radius of the inner PEC core is very small compared to the outer radius of the coating is the impact of rotation noticeable. Given the same coating, high backscattering can be achieved by requiring the PEC radius to be small. It can also be observed that the oscillation appears quite regular especially after $a > 0.4b$, though a little amplification is shown. Since C_B has been normalized by the outer radius b, the electric size of the backscattering cross section can change within the range (50,120) when a/b is sufficiently large. Further results show that the difference due to the angular velocity at $a < 0.15b$ and the oscillation can be suppressed by increasing the loss in the coating. As a particular example, we consider a highly lossy coating material with loss tangent of 6. As shown in Fig. 11, when the ratio is below 0.9, the backscattering is a constant value, which is independent of the radii ratio and rotation velocity. Small differences occur only when the inner PEC radius is getting very close to the outer radius.

If we consider the normalized velocity of $\beta_2 = \pm 0.04$ for a large coated cylinder (e.g., several millimeters in physical radius and $kb = 20$), it actually implies that a very large value of angular speed Ω_2 is needed, which may be difficult to implement in the experimental setup. In fact, in the case of $kb = 20$ for example, the object is much bigger than the wavelength of the incident radiation. However, there are still some results in such cases. They indicate that, even if the shell is rotating at a high speed for physically thick cylinders $kb = 20$, the shift of resonance is not huge, no matter how the core-shell ratio is adjusted. Thus, if we rotate the rod at normal velocity, the far-field backscattering will certainly have no obvious change.

VI. CONCLUSION

In this paper, the enhancement in backscattering of a coated metamaterial cylinder is examined, and a nanocylinder will be highly observable if the core-coating ratio is properly adjusted so as to generate interface resonances. The shifted resonances due to rotation are presented through a full-wave analysis, and the effects of rotation are characterized. The control in the core-coating ratio is extensively investigated in order to achieve suppression or enhancement of the scattering. Both the anomalous far-field scattering diagram and near-field localization are explored and corresponding resonance mechanisms are discussed.

ACKNOWLEDGMENTS

The authors are grateful for financial support from the SUMMA Foundation in the U.S. and the French-Singaporean Merlion Project. Also, stimulating discussions with Dr. Sergei Tretyakov are greatly appreciated.

[1] R. W. P. King and T. T. Wu, *The Scattering and Diffraction of Waves* (Harvard University Press, Cambridge, MA, 1959).
[2] C. Yeh and Z. A. Kaprielian, Can. J. Phys. **41**, 143 (1963).
[3] H. C. Chen and D. K. Cheng, Appl. Sci. Res., Sect. B **11**, 442 (1965).
[4] J. R. Wait, *Electromagnetic Waves in a Stratified Media* (Pergamon, New York, 1962).
[5] L. D. Landau and E. M. Lifshitz, *Electrodynamics of Continuous Media* (Pergamon, Oxford, 1984).
[6] R. M. More and K. Kosaka, Phys. Rev. E **57**, 6127 (1998).
[7] C. W. Qiu, L. W. Li, H. Y. Yao, and S. Zouhdi, Phys. Rev. B **74**, 115110 (2006).

[8] C. W. Qiu, H. Y. Yao, L. W. Li, S. Zouhdi, and T. S. Yeo, J. Phys. A **40**, 5751 (2007).
[9] H. Y. Yao, L. W. Li, C. W. Qiu, Q. Wu, and Z. N. Chen, Radio Sci. **42**, RS2006 (2007).
[10] C. W. Qiu, H. Y. Yao, S. N. Burokur, S. Zouhdi, and L. W. Li IEICE Trans. Commun. **E90-B**, 2423 (2007).
[11] J. B. Pendry, D. Schurig, and D. R. Smith, Science **312**, 1780 (2006).
[12] S. A. Cummer, B. I. Popa, D. Schurig, D. R. Smith, and J. B. Pendry, Phys. Rev. E **74**, 036621 (2006).
[13] A. Alù and N. Engheta, Phys. Rev. E **72**, 016623 (2005).
[14] C. W. Qiu, H. Y. Yao, L. W. Li, S. Zouhdi, and T. S. Yeo, Phys. Rev. B **75**, 155120 (2007).
[15] C. W. Qiu, L. W. Li, T. S. Yeo, and S. Zouhdi, Phys. Rev. E **75**, 026609 (2007).
[16] X. M. Zhou and G. K. Hu, Phys. Rev. E **74**, 026607 (2006).
[17] A. Alù and N. Engheta, J. Appl. Phys. **97**, 094310 (2005).
[18] M. G. Silveirinha, A. Alù, and N. Engheta, Phys. Rev. E **75**, 036603 (2007).
[19] U. Leonhardt, Science **312**, 1777 (2006).
[20] A. Hendi, J. Henn, and U. Leonhardt, Phys. Rev. Lett. **97**, 073902 (2006).
[21] D. R. Smith, J. B. Pendry, and M. C. K. Wiltshire, Science **305**, 788 (2004).
[22] R. W. Ziolkowski and N. Engheta, *Electromagnetic Metamaterials: Physics and Engineering Applications* (John Wiley & Sons, New York, 2006).
[23] R. L. Fante and M. T. McCormack, IEEE Trans. Antennas Propag. **30**, 1443 (1968).
[24] K. J. Vinoy and R. M. Jha, *Radar Absorbing Materials: From Theory to Design and Characterization* (Kluwer Academic Publishers, Norwell, MA, 1996).
[25] D. L. Jaggard and N. Engheta, Electron. Lett. **25**, 173 (1989).
[26] D. L. Jaggard and N. Engheta, Electron. Lett. **26**, 1332 (1990).
[27] A. Alù and N. Engheta, IEEE Trans. Antennas Propag. **51**, 2558 (2003).
[28] J. J. Chen, T. M. Grzegorczyk, B. I. Wu, and J. A. Kong, J. Appl. Phys. **98**, 094905 (2005).
[29] A. Alù, N. Engheta, and R. W. Ziolkowski, Phys. Rev. E **74**, 016604 (2006).
[30] P. Alitalo, S. Maslovski, and S. Tretyakov, Phys. Lett. A **357**, 397 (2006).
[31] A. Sommerfeld, *Electrodynamics*, translated from the German by E. G. Ramberg (Academic Press, New York, 1964).
[32] J. V. Bladel, Proc. IEEE **64**, 301 (1976).
[33] B. S. Luk'yanchuk and V. Ternovsky, Phys. Rev. B **73**, 235432 (2006).